IEEE Access
Multidisciplinary ⋮ Rapid Review ⋮ Open Access Journal

Received 26 February 2025, accepted 17 March 2025, date of publication 27 March 2025, date of current version 7 April 2025.

Digital Object Identifier 10.1109/ACCESS.2025.3555531

RESEARCH ARTICLE

Error Rate Analysis of Quantum-Annealing-Aided Multi-User Detection in Power-Domain Nonorthogonal Multiple Access

KOUKI YONAGA[1], KENICHI TAKIZAWA[1], (Member, IEEE), AND MASARU INABA[2]
[1]Resilient ICT Research Center, National Institute of Information and Communications Technology (NICT), Sendai, Miyagi 980-0812, Japan
[2]Quantum Computing Business Department, NEC Corporation, Minato City 108-8001, Japan

Corresponding author: Kouki Yonaga (yonaga@nict.go.jp)

This work was supported by Japan's Ministry of Education, Culture, Sports, Science, and Technology (MEXT) Quantum Leap Flagship Program under Grant JPMXS0120319794.

ABSTRACT We present the error rate performance of quantum-annealing-aided multiuser detection (QA-aided MUD), a signal detection approach that combines quantum annealing (QA) with conventional iterative multiuser detection (MUD). This method utilizes QA to compute log-likelihood ratios (LLR), improving signal detection and enhancing connectivity in power-domain nonorthogonal multiple access (PD-NOMA) systems. However, owing to the limited computational resources of the QA hardware, a detailed error-rate analysis was not performed. In this study, we extend QA-aided MUD to digital annealing techniques and evaluate the error rate performance of uplink PD-NOMA systems. Block error rate (BLER) analysis demonstrates that QA-aided MUD outperforms the conventional successive interference cancellation (SIC) method when difference of received signal strength corresponding to devices at base station is small. Moreover, we revealed that tuning the annealing parameters is crucial to obtain such better BLER performance. Additionally, we conducted evaluation on a bit error rate (BER) with a few instances to compare the performance of the QA hardware and digital annealing techniques. The results indicate that signal detection can be achieved using all the annealing techniques. Finally, we present the latest challenges, including an over-the-air (OTA) experiment using QA-aided MUD.

INDEX TERMS Multi-user detection, power-domain nonorthogonal multiple access, quantum annealing.

I. INTRODUCTION

In recent decades, quantum annealing (QA) has evolved into an innovative computational technique. QA is a versatile algorithm for solving combinatorial optimization problems and efficiently exploring optimal solutions by leveraging quantum effects [1], [2], [3]. Several studies have shown that QA outperforms the classical simulated annealing (SA) [4], [5], [6]. Notably, the QA protocol was implemented on a real device known as the D-wave quantum annealer (D-Wave). D-wave provides solutions to optimization problems with ultrahigh speed and extremely low power consumption [7]. Owing to these advantages, D-Wave has been applied in various practical applications, such as traffic optimization [8], scheduling and logistics [9], machine learning [10], and finance [11]. Thus, advances in QA technology will have a significant impact on the society.

Signal processing techniques that utilize QA have been actively studied in wireless communications [12], [13], [14], [15]. Recently, a new quantum-digital hybrid method called QA-aided multi-user detection (MUD) was proposed [16]. MUD is one of crucial techniques to enhance capability of multiple access in radio systems, especially when nonorthogonal multiple access (NOMA) [17] is introduced. In particular, iterative MUD [18] has potential to enhance massive connectivity more effectively than successive interference cancellation (SIC) [19] since iterative MUD does not require any difference in received signal strength. However, one of drawbacks of iterative MUD is to require a significant computation load to calculate the log-likelihood

The associate editor coordinating the review of this manuscript and approving it for publication was Walid Al-Hussaibi.

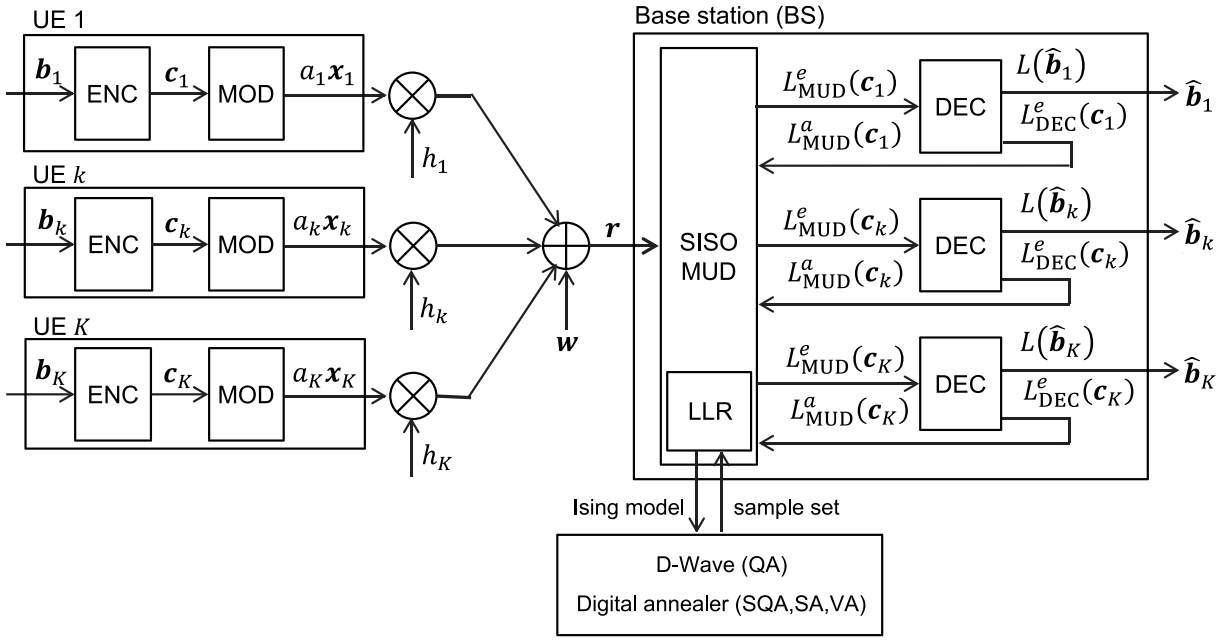

FIGURE 1. Block diagram of the uplink power-domain NOMA (UL PD-NOMA) with QA aided MUD.

ratio (LLR) accurately. Thus, we have developed QA-aided MUD to overcome this weak point, and shown that our method successfully reduce the computational speed by using D-wave. Furthermore, a previous study demonstrated that, in an uplink NOMA (UL-NOMA) system with seven connected users, QA-aided MUD achieves performance comparable to that of the original iterative MUD by analyzing bit error rate (BER) and convergence behavior [16]. Thus, QA-aided MUD has significant potential for enhancing future massive machine-type communication (mMTC) services. However, the computational resources of D-Wave are limited and the detailed error rate performance of QA-aided MUD, such as the block error rate (BLER), has not been clarified.

In this study, we examined the error rate performance of QA-aided MUD in uplink (UL) power-domain NOMA (PD-NOMA) systems [17]. Using both QA and digital annealing techniques, including simulated QA (SQA), simulated annealing (SA), and vector annealing (VA), we performed BLER analysis to assess the intrinsic performance of QA-aided MUD. Moreover, we evaluated the average BER in a few instances, comparing the performances of D-wave and digital annealing techniques. We further analyzed how the annealing parameters affected the error rate performance of QA-aided MUD. The contributions of this study are as follows:

- We extend the previously proposed QA-aided MUD to the digital annealing techniques and test it in PD-NOMA systems that does not introduce any other low-density signatures (e.g., interleaving [20]) except difference on received power at base station.
- Through BLER analysis using SQA and SA, we demonstrate that QA-aided MUD outperforms the conventional SIC when difference of received signal strength corresponding to devices at base station is small.
- We conduct evaluation on BER with a few instances using SQA, SA, VA, and D-Wave. We demonstrate that all annealers can achieve an error-free performance.
- We reveal that tuning the annealing parameters, especially the number of samplings, is crucial to obtain better error rate performance in QA-aided MUD.
- We present our latest challenge: demonstration of QA-aided MUD through an over-the-air (OTA) experiment.

The remainder of this paper is organized as follows. We describe our PD-NOMA system employing iterative MUD in Section II. We explain QA-aided MUD in Section III and then present a brief review of the annealing techniques in Section IV. In Section V, we present the results of BLER and BER analysis. We discuss these open issues and the future outlook in Sections VI and VII, respectively. Section VIII summarizes this study.

II. SYSTEM MODEL

A. UL PD-NOMA

Figure 1 illustrates a block diagram of the UL PD-NOMA systems, where a base station (BS) employs QA-aided MUD [16]. We denote the number of user equipment (UE) as K. We assume that all K UEs send data to BS simultaneously through the same frequency channel.

For the k-th UE, a sequence of information bits denoted by $\boldsymbol{b}_k = [b_k(1), \cdots, b_k(D)]$ is padded with cyclic redundancy check (CRC) bits and encoded using an error correction code (ENC). The codeword bits obtained with N bit lengths are represented by $\boldsymbol{c}_k = [c_k(1), \cdots, c_k(N)]$. The codeword

$\boldsymbol{c}_k$ is mapped to a sequence of modulated signals at modulator (MOD) with M constellation points as $\boldsymbol{x}_k = [x_k(1), \cdots, x_k(L)]$, where $L = N/\log_2(M)$. The received signal at BS, $\boldsymbol{r} = [r(1), \cdots, r(L)]$, is given by the superimposition of the transmitted signals as

$$r(i) = \sum_{k=1}^{K} h_k a_k x_k(i) + w(i). \tag{1}$$

We represent the amplitude of the transmitted signal from the k-th UE as a_k and the channel coefficient as $h_k = e^{j\phi_k}$. In addition, $\boldsymbol{w} = [w(1), \cdots, w(L)]$ represents the additive white Gaussian noise (AWGN) with zero mean and standard deviation σ_w. In error rate analysis, pathloss between BS and UEs are included in signal-to-noise ratio (SNR) determined by σ_w.

B. ITERATIVE MUD

Iterative MUD is a method for mitigating interuser interference at BS in which iterative processing between the MUD block and DECs is executed [18], [21], [22], [23], as shown in Fig. 1. We define the LLR corresponding to the n-th transmitted codeword bit from the k-th UE, $c_k(n)$, as follows:

$$L_{\mathrm{MUD}}(c_k(n)) = \log \frac{\Pr[c_k(n)=1|\boldsymbol{r}]}{\Pr[c_k(n)=0|\boldsymbol{r}]}. \tag{2}$$

Using Bayes' theorem, (2) can be rewritten as

$$\begin{aligned} L_{\mathrm{MUD}}(c_k(n)) &= \log \frac{\Pr[\boldsymbol{r}|c_k(n)=1]}{\Pr[\boldsymbol{r}|c_k(n)=0]]} + \log \frac{\Pr[c_k(n)=1]}{\Pr[c_k(n)=0]]} \\ &= L^e_{\mathrm{MUD}}(c_k(n)) + L^a_{\mathrm{MUD}}(c_k(n)). \end{aligned} \tag{3}$$

The first and second terms represent the external and a priori LLR, respectively. The second term $L^a_{\mathrm{MUD}}(c_k(n))$ was calculated from the feedback from the DEC. First, we set $L^a_{\mathrm{MUD}}(c_k(n)) = 0\ ^\forall n, k$. Equation (3) is expressed as follows:

$$L_{\mathrm{MUD}}(c_k(n)) = \log \frac{\sum_{\boldsymbol{x}\in\boldsymbol{X}^1_{k,n}} \Pr[\boldsymbol{r}|\boldsymbol{x}] \cdot \Pr[\boldsymbol{x}]}{\sum_{\boldsymbol{x}\in\boldsymbol{X}^0_{k,n}} \Pr[\boldsymbol{r}|\boldsymbol{x}] \cdot \Pr[\boldsymbol{x}]}, \tag{4}$$

where $\boldsymbol{X} = \{\boldsymbol{x}_1, \cdots, \boldsymbol{x}_K\}$ represents the set of transmitted signals from all UEs. Additionally, $\boldsymbol{X}^1_{k,n}$ and $\boldsymbol{X}^0_{k,n}$ denote the subsets $\boldsymbol{X}$ when $c_k(n) = 1$ and $c_k(n) = 0$, respectively. After obtaining $L_{\mathrm{MUD}}(c_k(n))$ based on (4), the extrinsic LLR can be computed using $L^e_{\mathrm{MUD}}(c_k(n)) = L_{\mathrm{MUD}}(c_k(n)) - L^a_{\mathrm{MUD}}(c_k(n))$ as shown in (3). Subsequently, $L^e_{\mathrm{MUD}}(c_k(n))$ is sent to the k-th DEC as an a priori LLR.

In the k-th DEC, the LLR of $c_k(n)$ is computed as

$$\begin{aligned} L_{\mathrm{DEC}}(c_k(n)) &= \log \frac{\Pr[c_k(n)=1|L^a_{\mathrm{DEC}}(c_k(n)]}{\Pr[c_k(n)=0|L^a_{\mathrm{DEC}}(c_k(n)]} \\ &= L^e_{\mathrm{DEC}}(c_k(n)) + L^a_{\mathrm{DEC}}(c_k(n)), \end{aligned} \tag{5}$$

where the first and second terms represent the extrinsic and a priori information, respectively, and $L^a_{\mathrm{DEC}}(c_k(n))$ is equivalent to $L^e_{\mathrm{MUD}}(c_k(n))$. The information bit sequence for the k-th UE, $\hat{\boldsymbol{b}}_k$, is estimated based on the signs of $L_{\mathrm{DEC}}(\boldsymbol{b}_k))$.

In each iteration, after decoding at DEC, error detection is executed by CRC. Subsequently, $L^e_{\mathrm{DEC}}(\boldsymbol{c}_k)$ is fed back to the MUD block as $L^a_{\mathrm{MUD}}(\boldsymbol{c}_k)$. The iterative MUD executes the exchange of the LLRs between MUD and DECs until all the information bit sequences pass the CRC-check or until the number of iterations reaches the maximum.

To perform iterative MUD, we must calculate $\Pr[\boldsymbol{r}|\boldsymbol{x}]$ in (4). As (1) shows, the probability can be expressed as $\Pr[\boldsymbol{r}|\boldsymbol{x}] = \prod_{i=1}^{L} \Pr[r(i)|\boldsymbol{x}(i)]$, where $\boldsymbol{x}(i) = [x_1(i), \cdots, x_K(i)]$. Because we consider an AWGN channel with block fading h_k, $\Pr[r(i)|\boldsymbol{x}(i)]$ is defined by a complex Gaussian distribution as

$$\Pr[r(i)|\boldsymbol{x}(i)] = \frac{e^{\frac{-1}{2\sigma_w^2}E(\boldsymbol{x}(i))}}{\sum_{\boldsymbol{x}(i)\in\boldsymbol{X}(i)} e^{\frac{-1}{2\sigma_w^2}E(\boldsymbol{x}(i))}}, \tag{6}$$

where $\boldsymbol{X}(i)$ denotes the set of possible values of $\boldsymbol{x}(i)$. Here, the energy $E(\boldsymbol{x}(i))$ in (6) is defined as

$$E(\boldsymbol{x}(i)) = \left\| r(i) - \sum_{k=1}^{K} h_k x_k(i) \right\|^2. \tag{7}$$

When we employ QPSK ($M = 4$), the computational complexity is $O(M^K) = O(4^K)$. Consequently, the computation time for (6) increased exponentially with an increase in K.

III. QA-AIDED MUD

A. OVERVIEW OF QA

QA is a metaheuristic method to solve optimization problems [1], [2]. A QA system comprises two parts: the target and the driver. The target part represents the optimization problem we aim to solve, whereas the driver part introduces quantum fluctuations and creates a superposition of all possible solution states. To initiate QA, we set the driver part as the dominant part and explored diverse solutions. Then, we gradually reduced the influence of the driver, guiding the system towards a solution. The time required for this process is called the annealing time T_{anneal}. When T_{anneal} is sufficiently long, and the system suffers no external interferences, it can reach an optimal solution. A previous study reported that QA outperformed classical simulated annealing under ideal conditions [4], [24].

B. D-WAVE QUANTUM ANNEALER

D-Wave is designed to solve the Ising-type energy function as

$$E_{\mathrm{Ising}}(z) = \sum_{i<j} J_{i,j} z_i z_j + \sum_i h_i z_j, \tag{8}$$

where $z_i = \{+1, -1\}$ and $\boldsymbol{z} = [z_1, \cdots, z_{N_{\mathrm{Ising}}}]$ represent the Ising variable and vector of Ising variables with N_{Ising} length, respectively. Unfortunately, the current D-Wave hardware cannot directly handle all types of Ising models due to limitations in the connectivity between quantum bits [25]. Consequently, the embedding and unembedding techniques are essential [26], [27], [28]. The embedding maps $E_{\mathrm{Ising}}(z)$ into a solvable format on D-Wave, and the umembedding

remaps QA results into the original Ising-format. Thus, D-Wave is available for arbitrary Ising models through the use of the embedding and unembedding.

Notably, D-Wave is a sampler rather than a solver. The QA system can achieve the lowest energy solution of $z^* = \mathrm{argmin}_z E_{\mathrm{Ising}}(z)$ if noise effects are absent and the annealing time is sufficiently long. However, random noise significantly affects actual quantum devices [29], [30]. Thus, the D-wave system generates various approximate solutions stochastically. In fact, previous studies have reported that samples obtained using D-Wave are distributed around the lowest-energy solution [31]. Here, we introduce the essential techniques to obtain lower-energy solutions: minimize-energy and greedy steepest method [32]. The minimized-energy method performs an unembedding process while computing the local Ising energy. The greedy steepest descent method recalculates the Ising energy and updates the obtained solutions. These methods are post-processing steps performed on digital computers after QA.

C. ISING MODEL FOR UL PD-NOMA

When we employing QPSK modulation ($M = 4$), the k-th user symbol can be represented with two Ising variables $z(i) = [z_k^{(1)}(i), z_k^{(2)}(i)]$ as $x_k(i) = (z_k^{(1)}(i) + jz_k^{(2)}(i))/\sqrt{2}$. Substituting this representation into (7), we obtain the Ising model for the UL PD-NOMA system as [16]

$$\begin{aligned} E(\boldsymbol{z}(i)) = &\sum_{k}^{N_{\mathrm{Ising}}} H_k^1 z_k^1(i) + H_k^2 z_k^2(i) \\ &+ \sum_{k<l}^{N_{\mathrm{Ising}}} J_{k,l}^{11}\left(z_k^1(i)z_l^1(i) + z_k^2(i)z_l^2(i)\right) \\ &+ \sum_{k<l}^{N_{\mathrm{Ising}}} J_{k,l}^{12}\left(-z_k^1(i)z_l^2(i) + z_k^2(i)z_l^1(i)\right), \end{aligned} \tag{9}$$

where $N_{\mathrm{Ising}} = \log(M)K = 2K$. The coefficients H_k^1, H_k^2, $J_{k,l}^{11}$, and $J_{k,l}^{12}$ are given by:

$$H_k^1 = -\sqrt{2}a_k\left\{\mathrm{Re}(r(i))\mathrm{Re}(h_k) + \mathrm{Im}(r(i))\mathrm{Im}(h_k)\right\} \tag{10}$$

$$H_k^2 = \sqrt{2}a_k\left\{\mathrm{Re}(r(i))\mathrm{Im}(h_k) - \mathrm{Im}(r(i))\mathrm{Re}(h_k)\right\} \tag{11}$$

$$J_{k,l}^{11} = a_k a_l\left\{\mathrm{Re}(h_k)\mathrm{Re}(h_l) + \mathrm{Im}(h_k)\mathrm{Im}(h_l)\right\} \tag{12}$$

$$J_{k,l}^{12} = a_k a_l\left\{\mathrm{Re}(h_k)\mathrm{Im}(h_l) - \mathrm{Im}(h_k)\mathrm{Re}(h_l)\right\}, \tag{13}$$

respectively.

D. LLR APPROXIMATION WITH QA

After sending the Ising model to the D-Wave cloud service, QA is performed. As noted, because the current quantum annealer is treated as a sampler, D-wave returns a set of solutions referred to as a "sample set." Each sample mainly includes the following information.

- Spin pattern $z(i)$, e.g. $z(i) = [+1, -1, -1, \cdots,]$
- Ising energy $E(z(i))$

We denote the set of spin patterns obtained from the sample set as $\mathcal{Z}_{\mathrm{DW}}(i)$ and approximate $\Pr[r(i)|\boldsymbol{x}(i)]$ as follows:

$$\Pr_{\mathrm{DW}}[r(i)|\boldsymbol{z}(i)] = \frac{e^{\frac{-1}{2\sigma_w^2}E(\boldsymbol{z}(i))}}{\sum_{z(i)\in\mathcal{Z}_{\mathrm{DW}}(i)} e^{\frac{-1}{2\sigma_w^2}E(\boldsymbol{z}(i))}}. \tag{14}$$

Here, we replace $\boldsymbol{x}(i)$ with $\boldsymbol{z}(i)$ in the above equation. The key aspect of QA-aided MUD is a reduction of computational load to obtain the Gaussian distribution by introducing QA. Calculating $\Pr_{\mathrm{DW}}[r(i)|\boldsymbol{z}(i)]$ requires the computational complexity $O(|\mathcal{Z}_{\mathrm{DW}}|)$, where $|\cdot|$ means the size of a set, whereas $\Pr[r(i)|\boldsymbol{x}(i)]$ does $O(M^K)$. Furthermore, $|\mathcal{Z}_{\mathrm{DW}}|$ strongly depends on the annealing parameters, such as the number of samplings in QA. Consequently, QA-aided MUD can potentially accelerate iterative MUD by tuning the annealing parameters.

IV. OTHER ANNEALING TECHNIQUES

A. OVERVIEW

In the previous study, QA-aided MUD was proposed based on using QA on D-wave. However, digital annealing techniques are stochastic algorithms; therefore, we can apply digital techniques such as SQA, SA, and VA to approximate $\Pr[r(i)|\boldsymbol{x}(i)]$. Table 1 summarizes the characteristics of each annealing technique.

1) SQA

SQA is a classical algorithm used to simulate the QA processes on digital computers. The basic principle of SQA is to map a QA system to a classical system and explore solutions based on Monte Carlo algorithms [4]. Thus, SQA utilizes a statistical approach to replicate the probabilistic nature of quantum mechanics and its time evolution. Crossen and Harrow reported that SQA can search for solutions more efficiently than SA or QA [33].

2) SA

SA is a probabilistic algorithm for searching for optimal solutions to optimization problems [34]. This method utilizes the thermal fluctuations derived from the physical annealing process in metallurgy. The SA algorithm starts at a high temperature, allowing the system to explore diverse solutions. As the temperature decreases, the system gradually converges to an optimal or near-optimal solution. If the SA process is performed with a sufficiently slow decrease in temperature, the system can reach an optimal solution.

3) VA

VA, also referred to as a quantum-inspired digital annealer, is a supercomputing system developed by NEC Corporation [35]. The basic principle of VA is nearly the same as that of SA; however, its software incorporates the proprietary algorithm of NEC on the vector supercomputer "SX-Aurora TSUBASA." Note that VA is a supercomputer designed to solve large-scale problems and its execution incurs a computational overhead.

TABLE 1. Summary on annealing techniques.

Method	Mechanism	Implementation	Parameters	Complexity or Time
QA (core sampling)	quantum fluctuation	D-Wave quantum device	$N_{\text{samp}}, T_{\text{anneal}}$	$N_{\text{samp}}(T_{\text{anneal}} + T_{\text{read}} + T_{\text{delay}})$
SQA	quantum fluctuation	digital computer	$N_{\text{samp}}, N_{\text{sweep}}, N_{\text{Trotter}}$	$N_{\text{Ising}}^2 \times N_{\text{samp}} \times N_{\text{sweep}} \times N_{\text{Trotter}}$
SA	thermal fluctuation	digital computer	$N_{\text{samp}}, N_{\text{sweep}}$	$N_{\text{Ising}}^2 \times N_{\text{samp}} \times N_{\text{sweep}}$
VA	thermal fluctuation	SX-Aurora TSUBASA	$N_{\text{samp}}, N_{\text{sweep}}$	$N_{\text{Ising}}^2 \times N_{\text{samp}} \times N_{\text{sweep}}$

B. ANNEALING PARAMETERS

The representative annealing parameters are summarized as follows [32], [36].

- N_{samp}: The number of samplings indicates how many times the annealing process is performed. While increasing N_{samp} extends the computation time, it also enhances the diversity of acquired samples, improving the likelihood of obtaining lower-energy solutions.
- T_{anneal}: The annealing time of QA. A longer T_{anneal} ideally increases the likelihood of finding the optimal solution; however, it also extends computation time and makes the QPU more susceptible to external interferences [3].
- N_{sweep}: The number of sweeps refers to the number of divisions used when decreasing the temperature or quantum effects during the annealing process. As N_{sweep} increases, the annealing process slows down, but the accuracy of the results improves [36].
- N_{Trotter}: The number of Trotter steps is a unique parameter in SQA that governs the mapping of a quantum system to a classical one. As N_{Trotter} increases, the classical system more accurately reproduces the original quantum system [4].

These parameters play a crucial role in determining the accuracy and computation time of annealing techniques. Thus, we investigated the effects of the above parameters on QA-aided MUD.

C. COMPUTATIONAL COMPLEXITY AND COMPUTATION TIME

Table 1 lists the complexity of the digital annealing techniques and the computation time of QA in D-wave. The complexity of SQA is $O(N_{\text{Ising}}^2 N_{\text{samp}} N_{\text{sweep}} N_{\text{Trotter}})$, while that of SA and VA is $O(N_{\text{Ising}}^2 N_{\text{samp}} N_{\text{sweep}})$, where $N_{\text{Ising}} = \log(M)K$. The K^2 (or N_{Ising}^2) factor was derived by calculating the Ising energy during the annealing process. Because the QA operation on the D-Wave hardware does not involve digital processing, we consider the computation time instead of complexity. The core sampling time of QA is given as $O(N_{\text{samp}}(T_{\text{anneal}} + T_{\text{read}} + T_{\text{delay}}))$ [32], where T_{read} and T_{delay} are the readout and delay time, respectively. As shown in Table 1, the core computation time of D-wave includes only the annealing parameters, whereas the complexities of the digital methods depend on K. This indicates that the computation time of D-wave has little dependence on K, which was confirmed in [16]. Therefore, QA-aided MUD employing D-wave can potentially operate at high speeds even in large-K systems. Note that, however, the actual computation time in the D-Wave system includes various overheads derived from pre- and post-process as mentioned in Section III-A.

TABLE 2. Common system parameters in the numerical experiments.

Parameters	Values
Modulation scheme	QPSK ($M = 4$)
# of symbols L	216
# of information bits D	114 bits
CRC	8 bits
Error correction code	Turbo code (3GPP TS 36.212 [37])
Coding rate	1/3

TABLE 3. Annealers and its parameters in the numerical experiments.

Parameters	Values
D-Wave	Advantage Systems 6.4
SQA and SA	Openjij Library
Vector Annealer	NEC SX-Aurora TSUBASA
# of sampling N_{samp}	$\{10, 32, 100, 320, 1000\}$
# of sweeps N_{sweep}	$\{10, 18, 32, 56, 100\}$
Trotter number N_{Trotter}	$\{2, 3, 4, 5, 6\}$
Annealing time T_{anneal}	$\{0.5, 0.9, 1.6, 2.8, 5.0\}$ μs

V. NUMERICAL RESULTS

Table 2 lists the system parameters used in this study, which are mainly based on previous studies [16]. We employed the log-MAP algorithm [38]. Furthermore, we assume that the channel coefficients $\{h_k\}$ and the standard deviations of AWGN σ_w are ideally estimated at BS. The channel coefficient is $h_k = e^{j\phi_k}$, where ϕ_k is generated using a uniform distribution over $(0, 2\pi]$. The power of k-th UE, a_k, is assigned as $10^{-(k-1)\cdot\Delta/20}$, where Δ in decibels represents

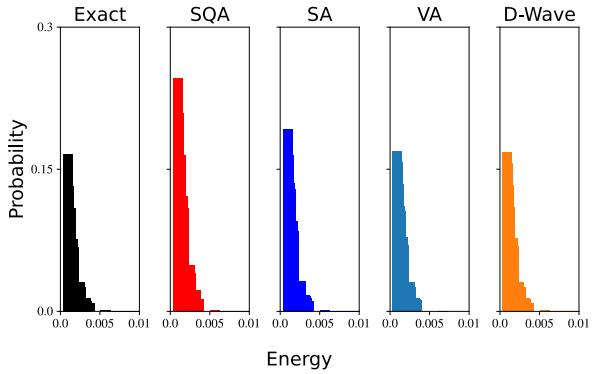

FIGURE 2. Examples of probability distributions for the received signal $r(1)$ for $K = 7$ at SNR = 25 dB.

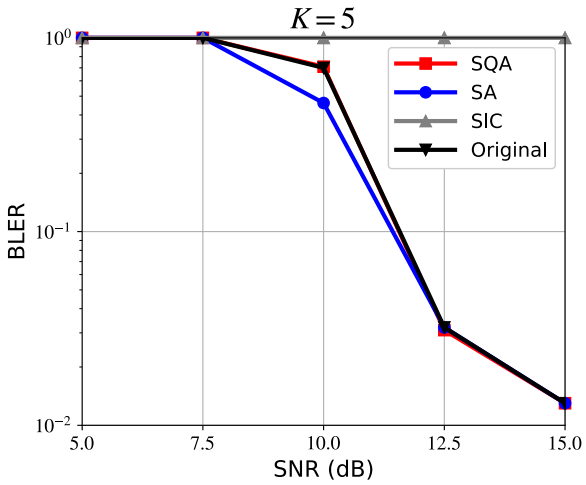

FIGURE 3. BLER curves for $\Delta = 1$ dB and $K = 5$ with $N_{\text{samp}} = 1000$, $N_{\text{sweep}} = 100$, and $N_{\text{Trotter}} = 4$.

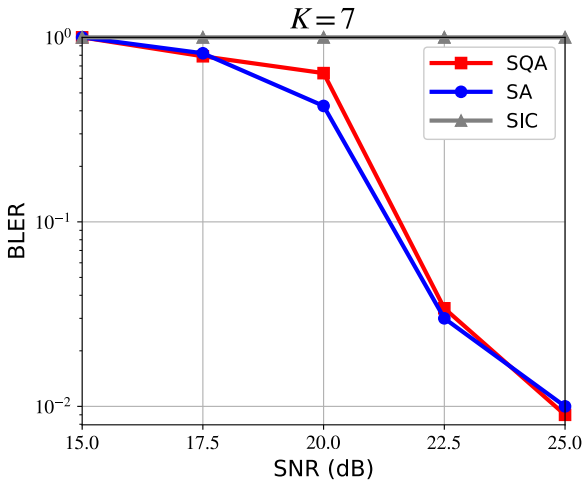

FIGURE 4. BLER curves for $\Delta = 1$ dB and $K = 7$ with $N_{\text{samp}} = 1000$, $N_{\text{sweep}} = 100$, and $N_{\text{Trotter}} = 4$.

the power difference that enhances multi-user detection in PD-NOMA.

Table 3 lists the annealers used and their parameters. The D-Wave system used was Advance System 6.4, and we employed the greedy method for post-processing. The annealing time T_{anneal} is $\{0.5, 0.89, 1.58, 2.81, 5.0\}$ μs. For SQA and SA, we used the OpenJij library [36] and NEC's SX-Aurora TSUBASA was employed as VA. We set the number of samplings as $N_{\text{sample}} = \{10, 32, 100, 320, 1000\}$, the number of sweeps as $N_{\text{sweep}} = \{10, 18, 32, 56, 100\}$, and the trotter number $N_{\text{Trotter}} = \{2, 3, 4, 5, 6\}$. The annealing time T_{anneal} was set as $\{0.5, 0.9, 1.6, 2.8, 5.0\}$ μs.

To obtain the performance of BLER over all UEs, we generated 1000 instances, including $\{\boldsymbol{b}_k\}$, $\{h_k\}$ and $\boldsymbol{w}$. The same generated 1000 instances were used across all the experiments using SQA, SA, and SIC. Additionally, the BLER values presented in this paper were calculated for a single transmission, meaning that no retransmission schemes, such as hybrid automatic retransmission request (HARQ) [39], were introduced. The average BER across all UEs was obtained using five instances for SQA, SA, VA, and D-wave.

A. COMPARING DISTRIBUTIONS

Figure 2 illustrates examples of the probability distribution for the first received signal $r(1)$ in $K = 7$ at SNR = 25 dB. "Exact" denotes the result exactly computed from (6), and the other results are calculated based on (14). We set $N_{\text{samp}} = 1000$, $N_{\text{sweep}} = 100$, and $T_{\text{anneal}} = 0.5$ μs. The distribution obtained using Exact is primarily localized around the lowest-energy solution and broadens towards the high-energy regions. Although the distributions obtained by the annealing techniques differed quantitatively from those obtained by Exact, they successfully reproduced the overall trends.

B. BLER ANALYSIS

1) BLER VERSUS SNR

Figure 3 illustrates the BLER performance for $\Delta = 1$ dB obtained using SQA and SA for $K = 5$. Here, we set $N_{\text{samp}} = 1000$, $N_{\text{sweep}} = 100$, and $N_{\text{Trotter}} = 4$. For comparison, we show the results obtained by SIC as a conventional method [19] and the original iterative MUD [18] denoted as "Original." The BLERs of Original, SQA, and SA decreased with an increase in SNR, whereas the BLER of SIC did not improve, even in high-SNR regions. Such BLER performance of SIC, where the improvement in BLER with increasing SNR is not observed, has also been reported in the previous study [19]. This is because the power difference given by Δ is insufficient to decode the first UE. Furthermore, SQA and SA exhibited BLER performances comparable to those of the original. Fig. 4 shows the BLER curves of SQA, SA, and SIC for $K = 7$. When $K = 7$, QA-aided MUD could successfully perform signal detection, which was difficult for the original iterative MUD. The BLER curves demonstrate that SQA and SA significantly outperform SIC over all SNRs

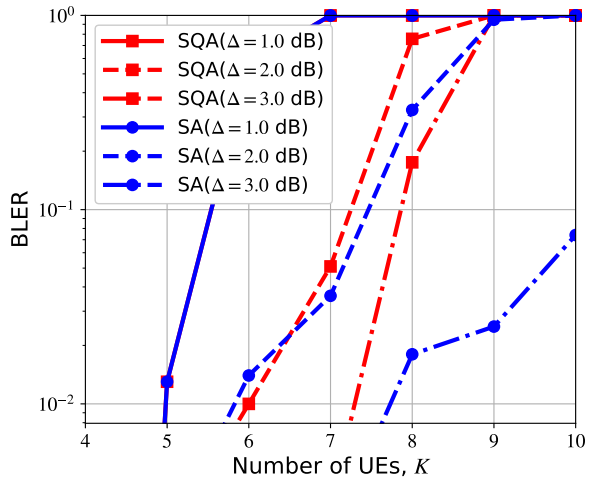

FIGURE 5. BLER vs. K with $\Delta = \{1, 2, 3\}$ dB, where SNR = 15 dB.

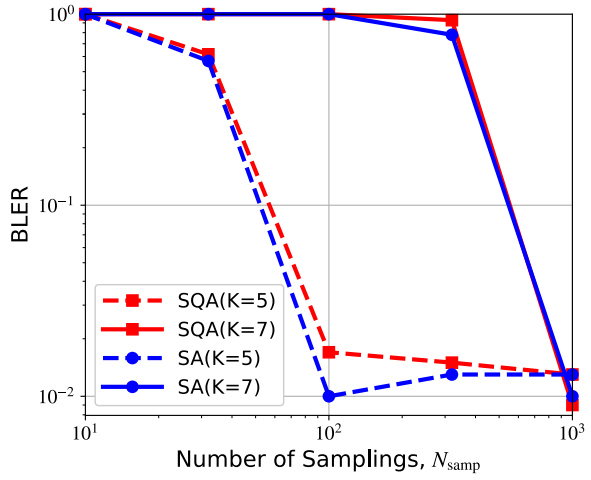

FIGURE 6. BLER versus N_{samp} with $N_{\text{sweep}} = 100$, $N_{\text{Trotter}} = 4$, and $\Delta = 1$ dB, where SNR = 15 and 25 dB for $K = 5$ and 7, respectively.

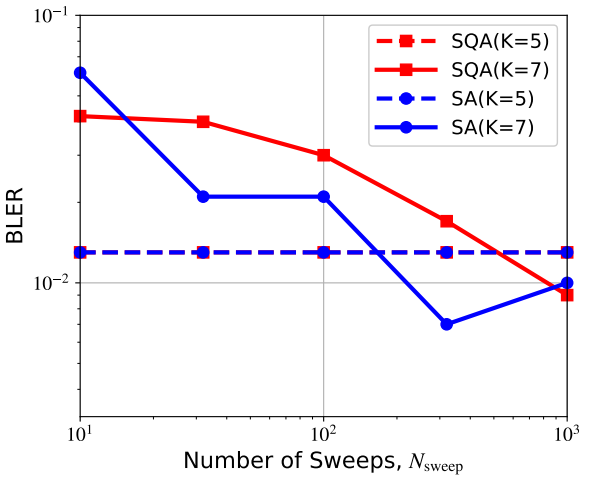

FIGURE 7. BLER versus N_{sweep} with $N_{\text{samp}} = 1000$, $N_{\text{Trotter}} = 4$, and, and $\Delta = 1$ dB, where SNR = 15 and 25 dB for $K = 5$ and 7, respectively.

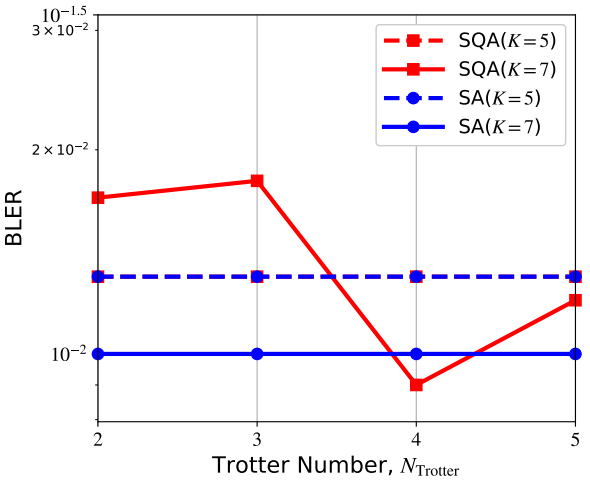

FIGURE 8. BLER versus N_{Trotter} with $N_{\text{samp}} = 1000$, $N_{\text{sweep}} = 100$, and $\Delta = 1$ dB, where SNR = 15 and 25 for $K = 5$ and 7, respectively.

for $K = 7$. Furthermore, SQA and SA have comparable performance for $K = 5$ and 7.

Figure 5 illustrates the K-dependence of the BLERs using SQA and SA. The SNR was set to 15 dB and the results are shown with a power difference $\Delta = \{1, 2, 3\}$ dB. The results demonstrate that the BLER performance of SQA and SA degrades with an increase in K. However, when Δ increases, the BLERs of both annealers improve. Notably, the BLER performance of the SA remained below 10^{-1} over all K values when $\Delta = 3$ dB. These results indicate that QA-aided MUD can potentially detect transmitted signals from up to 10 UEs when Δ is sufficiently large.

2) BLER VERSUS ANNEALING PARAMETERS

Figure 6 shows the N_{samp}-dependence on the BLER performance of QA-aided MUD with $\Delta = 1$ dB, where $N_{\text{sweep}} = 100$ and $N_{\text{Trotter}} = 4$. We set SNR=15 dB for $K = 5$ and SNR=25 dB for $K = 7$. For $K = 5$, the BLERs improve significantly when $N_{\text{samp}} \geq 100$. Furthermore, the BLERs show a sharp improvement at $N_{\text{samp}} = 1000$ for $K = 7$. The results indicate that a larger N_{samp} is necessary for achieving accurate BLER performance with an increase in K. Fig. 7 illustrates the BLER performance versus the number of sweeps, N_{sweep}. For $K = 5$, no N_{sweep}dependence was observed; however, the BLERs gradually improved with increasing N_{sweep} for $K = 7$. We show the dependence of the BLER on N_{Trotter} in Fig. 8, where $N_{\text{samp}} = 1000$ and $N_{\text{sweep}} = 100$. Although N_{Trotter} is a unique parameter for SQA, we present the results obtained using the SA for comparison. The results show that the BLER reached a minimum at $N_{\text{Trotter}} = 4$ for $K = 7$, whereas no improvement was observed for $K = 5$.

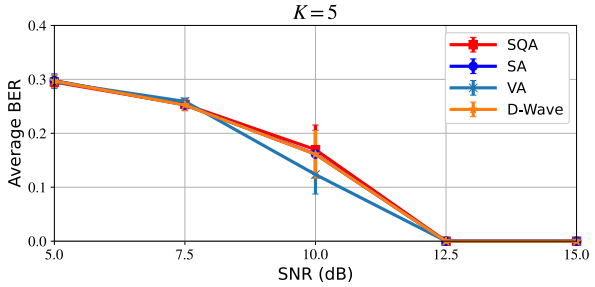

FIGURE 9. Average BER performance for $K = 5$ with $N_{\text{samp}} = 1000$, $N_{\text{sweep}} = 10$, $N_{\text{Trotter}} = 4$, $T_{\text{anneal}} = 0.5$ μs, and $\Delta = 1$ dB.

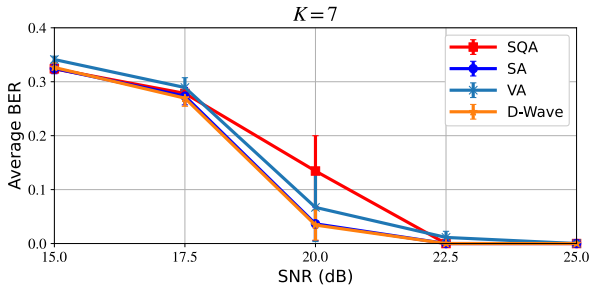

FIGURE 10. Average BER performance for $K = 7$ with $N_{\text{samp}} = 1000$, $N_{\text{sweep}} = 100$, $N_{\text{Trotter}} = 4$, $T_{\text{anneal}} = 0.5$ μs, and $\Delta = 1$ dB.

We summarize the effects of the annealing parameters on QA-aided MUD. As shown in Fig. 6, increasing N_{samp} significantly improves the BLER performance of QA-aided MUD. This improvement is because we can obtain divergent solutions and reproduce $\Pr[r|\boldsymbol{x}]$ accurately when N_{samp} is sufficiently large. Further, increasing N_{sweep} enhances the BLER performance, although its impact is less significant compared to N_{samp}. For SQA, an appropriate N_{Trotter} slightly improves performance. Consequently, we demonstrate that N_{samp} has the most significant effect on the BLER performance of QA-aided MUD.

C. COMPARISON OF BER AMONG DIFFERENT ANNEALING TECHNIQUES

1) BER VS SNR

Figure 9 and 10 illustrate the BER performance using SQA, SA, VA, and D-Wave for $K = 5$ and 7, respectively. Here, the average BER was calculated using only a few instances; therefore, we show the results using error bars. We set $N_{\text{samp}} = 1000$, $N_{\text{Trotter}} = 4$, and $T_{\text{anneal}} = 0.5$ μs, and N_{sweep} is set to be 10 and 100 for $K = 5$ and 7, respectively. For $K = 5$, all BERs gradually decreased with an increase in SNR, reaching zero at SNR = 12.5 dB. For $K = 7$, all annealers achieved error-free performance at SNR = 25 dB. The results demonstrate that D-Wave and VA exhibit performances comparable to those of SQA and SA.

2) BER VS ANNEALING PARAMETERS

Figure 11 illustrates the dependence of the average BER on N_{samp}. The annealing time T_{anneal} was 0.5 μs, and we set

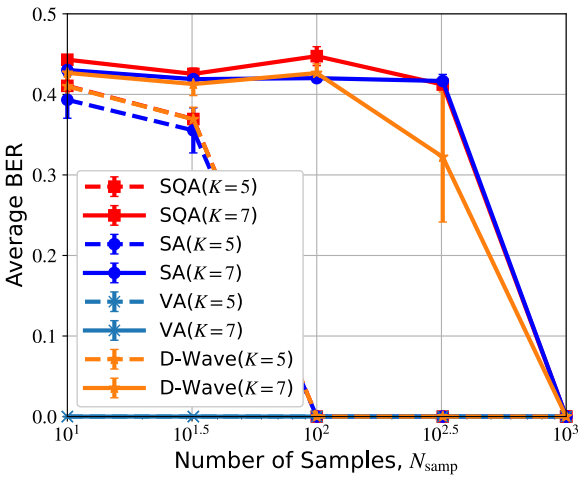

FIGURE 11. Average BER versus N_{samp} with $N_{\text{sweep}} = 100$, $N_{\text{Trotter}} = 4$, $T_{\text{anneal}} = 0.5$ μs, and $\Delta = 1$ dB, where SNR = 15 and 25 dB for $K = 5$ and 7, respectively.

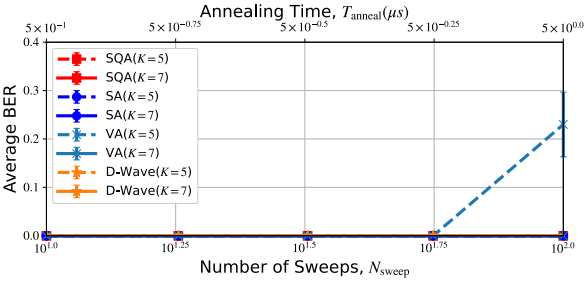

FIGURE 12. Average BER versus N_{sweep} and T_{anneal} with $N_{\text{samp}} = 1000$ and $\Delta = 1$ dB, where SNR = 15 and 25 dB for $K = 5$ and 7, respectively.

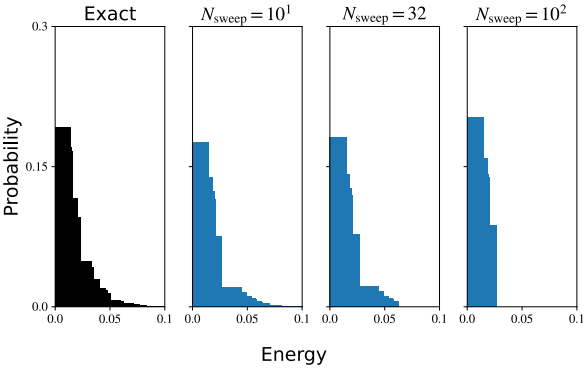

FIGURE 13. Comparison of the distributions for $K = 5$ obtained using the VA with $N_{\text{sweep}} = \{10, 32, 100\}$ and $\Delta = 1$ dB.

$N_{\text{sweep}} = 10$ and 100 for $K = 5$ and 7, respectively. For $K = 5(7)$, the BERs of SQA, SA, and D-Wave improve with an increase in N_{samp}, reaching BER = 0 at $N_{\text{samp}} = 100(1000)$. However, the BER of VA shows no dependence on N_{samp}, achieving an error free performance even with $N_{\text{samp}} = 10$.

Figure 12 displays the average BER as a function of N_{sweep} and T_{anneal}, where $N_{\text{samp}} = 1000$. The BERs of the D-wave remained at zero regardless of T_{anneal} for $K = 5$ and 7. Furthermore, the BER performance of VA shows no dependence on N_{sweep} for $K = 7$, whereas it degrades significantly at $N_{\text{sweep}} = 100$ for $K = 5$. Here, we further investigate the N_{sweep}-dependence of VA. Fig. 13 illustrates examples of the distribution for $K = 5$, which are obtained by VA with $N_{\text{sweep}} = \{10, 32, 100\}$. For comparison, we show the exactly calculated distribution. When $N_{\text{sweep}} = 10$, the distribution of VA is agreed with the exact result. However, as N_{sweep} increases, the distribution in the high-energy regions disappears and becomes concentrated around the lowest-energy solution. In general, the larger N_{sweep}, the more accurate the digital annealing techniques become. That is, the probability distribution becomes concentrated in the lower-energy regions because the likelihood of reaching the optimal solution increases. Consequently, the annealing results of VA were overly accurate and failed to reproduce the exact distribution when N_{sweep} for $K = 5$. To avoid this performance degradation, careful tuning of N_{sweep} is required for VA.

VI. DISCUSSION

A. ADVANTAGES OF QA-AIDED MUD

We highlight the differences between QA-aided MUD and other schemes. Current MUD techniques primarily rely on linear detection methods, such as linear minimum mean-square error (LMMSE), zero forcing (ZF), and maximal ratio combining (MRC) detectors. In particular, for coded NOMA schemes like interleave division multiple access (IDMA) [20], the LMMSE detector can achieve optimal MUD performance. However, these techniques require additional implementations on the transmitter (Tx) side, such as using an interleaver. Conversely, QA-aided MUD performs signal detection solely based on signal power differences between users without introducing additional functionality. Thus, QA-aided MUD eliminates the need for complex Tx-side implementations, providing a significant advantage in practical applications.

Furthermore, the key aspect of QA-aided MUD is its ability to efficiently compute the LLR from samples obtained through annealing techniques, making it widely applicable in digital communication technologies. For example, we utilized turbo coding in this study; however, the method can be extended to other coding schemes, such as low-density parity-check (LDPC) codes or Polar codes.

B. CHALLENGES

We discuss the computational complexity and computation time of the annealing techniques. The complexities of SQA, SA, and VA depend on K^2 as shown in Table 1, whereas that of LMMSE detector is $O(K^3)$. However, the complexities of the digital annealers depend not only on K but also on annealing parameters such as N_{samp}, N_{sweep}, and N_{Trotter}. Furthermore, the numerical results demonstrated that these annealing parameters significantly influenced the BLER and BER performances of QA-aided MUD. Therefore, an efficient method for tuning annealing parameters is necessary to balance the required accuracy and computation time.

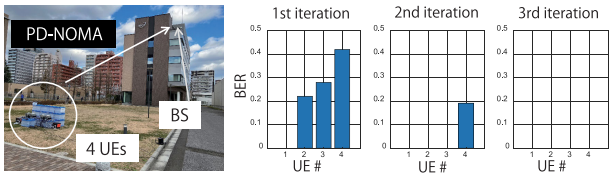

FIGURE 14. Demonstration of the QA-aided MUD with D-wave in UL PD-NOMA ($K = 4$ and $\Delta = 3$ dB in average).

For D-Wave, the QA sampling time depends on the annealing parameters; therefore, the computation time can remain constant, even as K increases. However, as discussed in Section III-B, D-Wave involves pre- and post-processing steps such as embedding, unembedding, and the greedy steepest descent method. These additional steps introduce significant overhead, thereby increasing the total computation time of QA-aided MUD. The recent development of low-noise hardware with new architectures has gradually mitigated this overhead [40]. Thus, with advancements in D-Wave, QA-aided MUD will be further accelerated.

Finally, we discuss the performance of VA. The numerical results show that QA-aided MUD using VA can reach an error-free performance with small N_{samp} or small N_{sweep}. Furthermore, a CPU version of the VA has recently been released, which significantly reduces the computation overhead in its execution. Thus, VA has great potential for enhancing the accuracy and computation speed of QA-aided MUD.

VII. FUTURE OUTLOOK

One of the challenges in realizing a massive communication system with the proposed QA-aided MUD is related to implementation. To demonstrate the feasibility of QA-aided MUD in a static environment, we applied it to PD-NOMA through OTA experiments. A photograph of the experiment is shown in Fig. 14. The setup for this experiment was the same as that shown in Fig. 1, with four UEs ($K = 4$) and a BS equipped with a single antenna. The UL PD-NOMA signal used in this experiment had a frequency bandwidth of 1.4 MHz and a center frequency of 2295 MHz. The modulation and coding scheme (MCS) was the same as that shown in Table 2. The Δ value, which determines a_k, was set to 3 dB based on the results shown in Fig. 5. The transmit power control was manually applied by evaluating the channel state information derived from the reference signals transmitted by the UEs. The distance between the UEs and the BS was approximately 50 m. Under these conditions, the SNR for the UE transmitting at the highest power level was approximately 26 dB. Fig. 14 illustrates the evo lution of the average BER for each UE after each iteration in

QA-aided MUD. In this experiment, D-Wave was employed as the annealing technique. The OTA experiment confirmed that QA-aided MUD successfully achieved signal separation in UL PD-NOMA. In UL PD-NOMA, the transmitted signals from each UE undergo individual distortions owing to radio propagation characteristics such as delay spread and Doppler shift in mobile channels. Becau se compensating for these distortions at the BS is not straightforward, an open problem remains in identifying an efficient compensation method that integrates both QA and digital computing.

VIII. SUMMARY

We extended the previously reported QA-aided MUD to digital annealing techniques and evaluated its error-rate performance in UL PD-NOMA. Through BLER analysis using SQA and SA, we demonstrated that QA-aided MUD significantly outperformed conventional SIC through the BLER analysis using SQA and SA. Additionally, we conducted a BER analysis using SQA, SA, VA, and D-Wave with a limited number of instances. The results indicated that the signal detection was achived across all annealers in high SNR regions. Furthermore, we demonstrated that annealing parameters, particularly the number of samplings, significantly impacted the BLER and BER performances of QA-aided MUD. These findings suggest that VA holds strong potential for enhancing the performance of QA-aided MUD. Finally, we present the results of an OTA experiment using QA-aided MUD.

REFERENCES

[1] T. Kadowaki and H. Nishimori, "Quantum annealing in the transverse ising model," *Phys. Rev. E, Stat. Phys. Plasmas Fluids Relat. Interdiscip. Top.*, vol. 58, no. 5, pp. 5355–5363, Nov. 1998.

[2] P. Hauke, H. G. Katzgraber, W. Lechner, H. Nishimori, and W. D. Oliver, "Perspectives of quantum annealing: Methods and implementations," *Rep. Prog. Phys.*, vol. 83, no. 5, May 2020, Art. no. 054401.

[3] A. Rajak, S. Suzuki, A. Dutta, and B. K. Chakrabarti, "Quantum annealing: An overview," *Phil. Trans. Roy. Soc. A, Math., Phys. Eng. Sci.*, vol. 381, no. 2241, Jan. 2023, Art. no. 20210417.

[4] G. E. Santoro, R. Martoňák, E. Tosatti, and R. Car, "Theory of quantum annealing of an ising spin glass," *Science*, vol. 295, no. 5564, pp. 2427–2430, Mar. 2002.

[5] R. Martoňák, G. E. Santoro, and E. Tosatti, "Quantum annealing of the traveling-salesman problem," *Phys. Rev. E, Stat. Phys. Plasmas Fluids Relat. Interdiscip. Top.*, vol. 70, no. 5, Nov. 2004, Art. no. 057701.

[6] C. Baldassi and R. Zecchina, "Efficiency of quantum vs. Classical annealing in nonconvex learning problems," *Proc. Nat. Acad. Sci. USA*, vol. 115, no. 7, pp. 1457–1462, Feb. 2018.

[7] C. McGeoch and P. Farré, "The D-Wave advantage system: An overview," Wave Syst. Inc., Burnaby, BC, Canada, Tech. Rep. 14-1049A-A, 2020.

[8] F. Neukart, G. Compostella, C. Seidel, D. von Dollen, S. Yarkoni, and B. Parney, "Traffic flow optimization using a quantum annealer," *Frontiers ICT*, vol. 4, p. 29, Dec. 2017.

[9] D. Venturelli, D. J. J. Marchand, and G. Rojo, "Quantum annealing implementation of job-shop scheduling," 2015, *arXiv:1506.08479*.

[10] R. K. Nath, H. Thapliyal, and T. S. Humble, "A review of machine learning classification using quantum annealing for real-world applications," *Social Netw. Comput. Sci.*, vol. 2, no. 5, p. 365, Sep. 2021.

[11] G. Rosenberg, P. Haghnegahdar, P. Goddard, P. Carr, K. Wu, and M. L. de Prado, "Solving the optimal trading trajectory problem using a quantum annealer," *IEEE J. Sel. Topics Signal Process.*, vol. 10, no. 6, pp. 1053–1060, Sep. 2016.

[12] M. Kim, D. Venturelli, and K. Jamieson, "Leveraging quantum annealing for large MIMO processing in centralized radio access networks," in *Proc. ACM Special Interest Group Data Commun.*, New York, NY, USA, Aug. 2019, pp. 241–255.

[13] S. Kasi, A. K. Singh, D. Venturelli, and K. Jamieson, "Quantum annealing for large MIMO downlink vector perturbation precoding," in *Proc. ICC-IEEE Int. Conf. Commun.*, Jun. 2021, pp. 1–6.

[14] S. Kasi, P. Warburton, J. Kaewell, and K. Jamieson, "A cost and power feasibility analysis of quantum annealing for NextG cellular wireless networks," *IEEE Trans. Quantum Eng.*, vol. 4, pp. 1–17, 2023.

[15] R. C. Kizilirmak, "Quantum annealing approach to NOMA signal detection," in *Proc. 12th Int. Symp. Commun. Syst., Netw. Digit. Signal Process. (CSNDSP)*, Jul. 2020, pp. 1–5.

[16] K. Yonaga and K. Takizawa, "Quantum annealing-aided multi-user detection: An application to uplink non-orthogonal multiple access," in *Proc. IEEE Int. Conf. Commun. (ICC)*, Jun. 2023, pp. 1357–1363.

[17] Y. Endo, Y. Kishiyama, and K. Higuchi, "Uplink non-orthogonal access with MMSE-SIC in the presence of inter-cell interference," in *Proc. Int. Symp. Wireless Commun. Syst. (ISWCS)*, Aug. 2012, pp. 261–265.

[18] H. Poor, "Iterative multiuser detection," *IEEE Signal Process. Mag.*, vol. 21, no. 1, pp. 81–88, Jan. 2004.

[19] M. Moriyama, A. Kurosawa, T. Matsuda, and T. Matsumura, "A study of parallel interference cancellation combined with successive interference cancellation for UL-NOMA systems," in *Proc. 24th Int. Symp. Wireless Pers. Multimedia Commun. (WPMC)*, Dec. 2021, pp. 1–6.

[20] L. Ping, L. Liu, K. Wu, and W. K. Leung, "Interleave division multiple-access," *IEEE Trans. Wireless Commun.*, vol. 5, no. 4, pp. 938–947, Apr. 2006.

[21] X. Wang and H. V. Poor, "Iterative (turbo) soft interference cancellation and decoding for coded CDMA," *IEEE Trans. Commun.*, vol. 47, no. 7, pp. 1046–1061, Jul. 1999.

[22] M. Moher, "An iterative multiuser decoder for near-capacity communications," *IEEE Trans. Commun.*, vol. 46, no. 7, pp. 870–880, Jul. 1998.

[23] C. Xu, Y. Hu, C. Liang, J. Ma, and L. Ping, "Massive MIMO, non-orthogonal multiple access and interleave division multiple access," *IEEE Access*, vol. 5, pp. 14728–14748, 2017.

[24] S. Morita and H. Nishimori, "Convergence theorems for quantum annealing," *J. Phys. A, Math. Gen.*, vol. 39, no. 45, pp. 13903–13920, Oct. 2006.

[25] K. Boothby, P. Bunyk, J. Raymond, and A. Roy, "Next-generation topology of d-wave quantum processors," D-Wave Syst., Burnaby, BC, Canada, Tech. Rep. 14-1026A-C, 2019.

[26] A. Lucas, "Hard combinatorial problems and minor embeddings on lattice graphs," *Quantum Inf. Process.*, vol. 18, no. 7, p. 203, Jul. 2019.

[27] S. Zbinden, A. Bärtschi, H. Djidjev, and S. Eidenbenz, "Embedding algorithms for quantum annealers with chimera and pegasus connection topologies," in *High Performance Computing*, P. Sadayappan, B. L. Chamberlain, G. Juckeland, and H. Ltaief, Eds., Cham, Swizerland: Springer, 2020, pp. 187–206.

[28] E. Pelofske, G. Hahn, and H. Djidjev, "Advanced unembedding techniques for quantum annealers," in *Proc. Int. Conf. Rebooting Comput. (ICRC)*, Dec. 2020, pp. 34–41.

[29] T. Zaborniak and R. de Sousa, "Benchmarking Hamiltonian noise in the D-Wave quantum annealer," *IEEE Trans. Quantum Eng.*, vol. 2, pp. 1–6, 2021.

[30] Z. Morrell, M. Vuffray, A. Y. Lokhov, A. Bärtschi, T. Albash, and C. Coffrin, "Signatures of open and noisy quantum systems in single-qubit quantum annealing," *Phys. Rev. Appl.*, vol. 19, no. 3, Mar. 2023, Art. no. 034053.

[31] K. Yonaga, M. J. Miyama, and M. Ohzeki, "Solving inequality-constrained binary optimization problems on quantum annealer," 2020, *arXiv:2012.06119*.

[32] D-Wave Syst. *D-Wave System Documentation*. Accessed: Mar. 30, 2025. [Online]. Available: https://docs.dwavesys.com/docs/latest/index.html

[33] E. Crosson and A. W. Harrow, "Simulated quantum annealing can be exponentially faster than classical simulated annealing," in *Proc. IEEE 57th Annu. Symp. Found. Comput. Sci. (FOCS)*, Oct. 2016, pp. 714–723.

[34] S. Kirkpatrick, C. D. Gelatt, and M. P. Vecchi, "Optimization by simulated annealing," *Science*, vol. 220, no. 4598, pp. 671–680, May 1983.

[35] Y. Yohei and M. Shintaro, "Vector engine processor of NEC's brand-new supercomputer sx-aurora tsubasa," in *Proc. 30th Symp. High Perform. Chips*, Aug. 2018, pp. 1–25.

[36] Jij Inc. (2019). *OpenJij*. [Online]. Available: https://github.com/OpenJij/OpenJij
[37] *Multiplexing and Channel Coding*, document TS36.212, 3GPP, 2022.
[38] B. Vucetic and J. Yuan, *Turbo Codes*. Boston, MA, USA: Kluwer, 2000.
[39] G. Berardinelli, S. R. Khosravirad, K. I. Pedersen, F. Frederiksen, and P. Mogensen, "Enabling early HARQ feedback in 5G networks," in *Proc. IEEE 83rd Veh. Technol. Conf. (VTC Spring)*, May 2016, pp. 1–5.
[40] E. Pelofske, "Comparing three generations of D-Wave quantum annealers for minor embedded combinatorial optimization problems," *Quantum Sci. Technol.*, vol. 10, no. 2, Feb. 2025, Art. no. 025025.

KOUKI YONAGA received the Ph.D. degree in physics from Tohoku University, in 2017.

He is currently a Researcher with the Resilient ICT Research Center, National Institute of Information and Communications Technology (NICT), Japan. His research interests include quantum annealing and its applications in wireless technology.

KENICHI TAKIZAWA (Member, IEEE) received the Ph.D. degree in engineering from Niigata University, in 2003. He joined the National Institute of Information and Communications Technology (NICT), in 2003. From 2011 to 2012, he stayed with Aalto University, Finland, as a Visiting Researcher. He received the Young Researcher's Award and the Best Paper's Award from IEICE, in 2006 and 2021, respectively.

MASARU INABA received the B.S. and M.S. degrees in physics from Osaka University, Osaka, Japan, in 1992 and 1994, respectively.

He joined NEC Corporation, Japan, in 1997, and has been working in various fields, including high-performance computing, mobile wireless communications, and quantum computing. His current research interest includes optimization problems.